Nuclear Instruments and Methods in Physics Research B 278 (2012) 34–41

Contents lists available at SciVerse ScienceDirect

Nuclear Instruments and Methods in Physics Research B

journal homepage: www.elsevier.com/locate/nimb

Detection of MeV particles from ultra-dense protium p(−1): Laser-initiated self-compression from p(1)

Frans Olofson, Leif Holmlid *

Atmospheric Science, Department of Chemistry and Molecular Biology, University of Gothenburg, SE-412 96 Göteborg, Sweden

ARTICLE INFO

Article history:
Received 6 December 2011
Received in revised form 24 January 2012
Available online 7 February 2012

Keywords:
MeV particles
Laser impact
Time-of-flight
Protons
Ultra-dense protium

ABSTRACT

Ultra-dense protium p(−1) is a condensed phase of hydrogen which has a shortest H–H bond distance of 3.7 pm. It is not identical in form to ultra-dense deuterium named d(−1) or D(−1). The MeV particles released from p(−1) under impact of a ns pulsed laser are studied with time-of-flight energy measurements using a fast plastic scintillator detector. A movable metal plate or foil is used to distinguish fast particles from energetic photons. The fast particles, mainly protons, are delayed by transmission through the plate or foil from the MeV range to 200–700 keV. Fast protons are ejected only after a 5–10 s induction period after the laser start, and only at high pulse rates, approaching 10 Hz. Particles with keV energies are ejected as late as several μs after the laser pulse. Nuclear processes are excluded in the p(−1) case and the laser intensity is quite low. It is concluded that laser-triggered self-compression from p(1) to p(−1) gives the high-energy particles.

1. Introduction

Nuclear fusion reactions can be caused by laser-initiated production of fast D atoms in ultra-dense deuterium called D(−1) or d(−1) [1,2]. The density of this ultra-dense material is close to 10^{29} cm^{-3} or 140 kg cm^{-3} as shown in several publications [3–13]. To better understand the details of the processes involved in the nuclear fusion in this material, we now also study the corresponding ultra-dense phase of hydrogen (protium) which is called p(−1). H(−1) is used to indicate both types of ultra-dense hydrogen, namely d(−1) and p(−1). High-energy particles and penetrating X-ray photons are observed from the laser impact on p(−1). If the small amount of deuterium in natural hydrogen is believed to give a negligible contribution, no fusion processes will be observed. One remote possibility for energy release in p(−1) is the transient formation of diprotons [14,15]. The energy released in their formation could be carried away by neighboring protons. This type of diproton formation might give rise to MeV protons. However, it is not generally believed that diprotons exist. Thus, other energetic processes in p(−1) give the high-energy particles. From a careful study, we conclude that the high-energy particles are released by laser-triggered self-compression of dense protium p(1) to ultra-dense protium p(−1). One important piece of evidence for this is the induction period observed for their formation.

Ultra-dense protium is named p(−1), since it is an inverted form of dense protium p(1), with orbital angular momentum $l = 1$ for the protons. It is similar to ultra-dense deuterium d(−1) or D(−1), which has been studied in several publications [3–13]. d(−1) is a quantum material [16] which may involve formation of vortices in a Cooper pair electron fluid as suggested by Winterberg [17,18]. It has a bond distance of 2.3 pm which may give a small rate of spontaneous fusion. The structure of d(−1) is given by long clusters D_{2N} with N integer formed by D–D pairs rotating around the vortex. p(−1) appears to be a quantum material with properties slightly different from d(−1). The bond distance in p(−1) is more variable and larger than 3.7 pm [7,19], and the cluster structure is not identical to that of d(−1). The density of p(−1) is smaller than 3×10^{28} cm^{-3} or 33 kg cm^{-3}.

2. Theory

Under impact of laser pulses, Coulomb explosions (CEs) [7] take place in the ultra-dense material p(−1) [19]. A typical CE involves only two ions formed in a p(−1) cluster. Excitation of one electron in the material may be sufficient to form these two ions. The potential energy between the two exposed charges is

$$W = \frac{e^2}{4\pi\varepsilon_0 d} \tag{1}$$

where d is the distance between the two ions. This energy is transformed almost completely to kinetic energy between the two ionic fragments during their mutual rapid repulsion. In ultra-dense deuterium, deuterons are observed with kinetic energy up to the kinetic energy release (KER) of 630 eV corresponding to $D^+ \leftrightarrow D^+D_N$ with N

* Corresponding author. Tel.: +46 31 7869076.
E-mail address: holmlid@chem.gu.se (L. Holmlid).

0168-583X/$ - see front matter © 2012 Elsevier B.V. All rights reserved.
doi:10.1016/j.nimb.2012.01.036

large [3–13]. Such processes will give nuclear fusion D + D in collisions between fast deuterons, albeit with a low probability.

In the material p(−1), similar CE processes exist. The bond distance in p(−1) is slightly larger than in d(−1), probably partly due to the fermion property of the protons. With the bond distance $\geqslant$3.7 pm, the CE energy is lower in p(−1), of the order of 390 eV instead of 630 eV for d(−1) [7,19]. In p(−1), no nuclear reactions are possible. Thus, it is expected that no fast particles will be observed by the main plastic scintillator detector which has a very low sensitivity at energies below a few keV. Photons in the X-ray range could possibly be formed at the laser impact, but acceleration of particles like protons to energies above a few keV is not expected.

The dense hydrogen material H(1) has been studied with a few different methods, mainly laser induced CE [20–22]. This form of hydrogen is a condensed material which is in rapid equilibrium with the ultra-dense material H(−1). Most studies on the transformation has been done for deuterium, observing the rapid transformation between d(1) and d(−1) [13]. An oscillation between these two forms of deuterium was indeed observed [9] and concluded to have a typical time of transformation of less than 0.1 s. The transformation between the two forms is probably driven by the lower energy of the material in the form H(−1). Since H(−1) is superfluid as shown experimentally for d(−1) [11], it is quite sensitive to energy input like absorption of light and seems to convert back to H(1) quite easily. Since H(−1) is a lower energy state, the transformation to H(−1) releases energy. As in most such processes observed in molecules and clusters, the preferred process to remove such excess energy is emission of a fast atom or small fragment. Since H(−1) is superfluid, the energy transport in the material is fast and an accumulation of the excess energy to a relatively small number of particles seems possible, giving an efficient energy pooling and ejection of protons (deuterons) with very high (MeV) energy. This type of process is suggested to be responsible for the high energy particles reported here.

3. Experimental

The main method used for the present studies is standard time-of-flight (TOF) and particle detection with a plastic scintillator and photo-multiplier (PMT). The layout of our experiment is shown in Fig. 1 [4]. A Nd:YAG laser with an energy of <300 mJ per each 5 ns long pulse at $\leq$10 Hz is used at 532 nm. The laser beam is focused with an f = 400 mm lens at the center of the UHV chamber. The laser intensity is $<10^{12}$ W cm^{-2} at the beam waist as calculated for a Gaussian beam. Close to the center of the apparatus, a potassium doped iron oxide catalyst sample [23,24] in the lower end of a vertical Pt tube is used as the emitter to produce p(−1) from hydrogen gas (N55, >99.9995%) at a pressure up to 1×10^{-5} mbar. The emitter is heated by an ac current through the Pt tube to a temperature <500 K. This source is described in detail elsewhere for the formation of ultra-dense deuterium [10]. The material p(−1) falls down onto a sloping metal surface (a Ta foil) a few mm below the source. This is the laser target in the experiments.

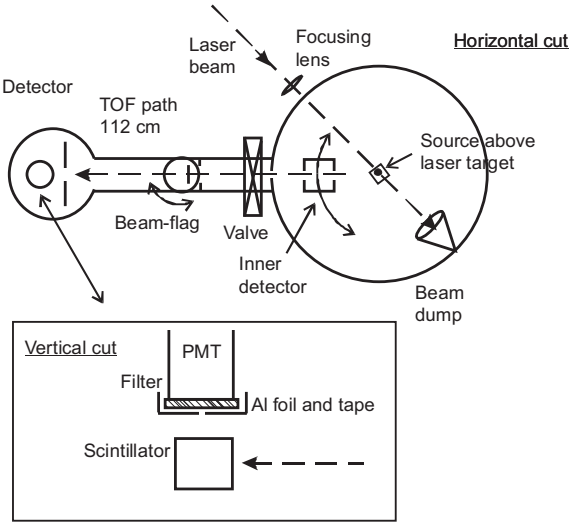

Fig. 1. Principle of the apparatus used. The source [10] has the catalyst emitter mounted at the bottom, close to the center of the chamber. The movable detector in the main chamber is here mainly used to select the position on the laser target below the source which is observed by the outer detector.

The main (outer) detector is at a distance of 112 ± 2 cm from the laser focus. Normally, a 5 cm thick plastic scintillator (BC-408, Saint-Gobain Crystals) with an entrance area of 20×26 mm^2 for the particle flux from the laser focus is used to detect high-energy particles and X-ray photons. It is covered by Al foil on the sides and the bottom surface to increase collection of the light from the scintillator. This scintillator is placed below the PMT such that the front surface of the scintillator is not visible to the PMT (no direct line-of-sight). In this way, the total signal due to fast massive particles which give scintillation within a short distance is reduced, thus decreasing the problem with too high signals in the PMT. The scintillator front is not covered with Al foil. The scintillators give blue photons which are observed by a PMT (EMI 9813B with single electron rise time of 2 ns) behind a 6 mm thick blue-violet glass filter (BG37, $T = 8 \times 10^{-6}$ at 532 nm). The PMT is mounted in a separate box in air outside a glass window in the vacuum wall. By this construction, stray laser photons and other photons generated by the laser at impact are removed. The PMT cathode area is covered by black plastic tape and also with Al foil, leaving only 1 mm^2 open for photons. The signal due to the 532 nm photons in the laser pulse is too small to be observed by the PMT. Since the whole experiment is inside a metal chamber, no stray or background light is of any importance. Closing the valve in the particle beam to the detector gives zero signal, as also found with Al foil coverage over the front part of the PMT. Thus, all external light leakage processes are removed. Here, the signal is mainly studied and recorded on a fast digital oscilloscope (Tektronix TDS 3032, 300 MHz) which displays the entire signal behavior. This is important due to the large signals often observed. A preamplifier (Ortec VT120A with gain 200×) is often used to decrease the time constant due to the cabling, but several tests without have been made. See further Section 5. A photodiode close to the laser gives a fast pulse which triggers the oscilloscope.

In the particle beam at a distance of 35 cm in front of the scintillator, a beam-flag can be moved into and out from the beam. The flag is a circular stainless steel plate frame (with a large circular opening) which is mounted with an offset on a rotating flange, and it is thus moved completely out of the beam when opened. On this flag, two or three 15 μm thick Al foils are mounted. To block the TOF tube cross section entirely when the flag is in place, a flat ring-shaped (annular) stainless steel plate is fitted into the tube in front of the foil holder. The surface of this plate is painted with Aquadag to remove reflections of light. Another selecting mechanism is used by moving a metal plate (with a vertical slit 3×20 mm^2 in the plate) to block the particle beam from the laser target. This metal plate is 3 mm thick and part of a separate device inside the main chamber (the inner detector in Fig. 1).

4. Results

We will here focus on the evidence of high-energy particles in the beam coming from the laser impact on the target. We will

show that an intensity is observed at a TOF corresponding to MeV particles, and that this intensity can be delayed by inserting either the beam-flag or the inner detector plate in the flux to the detector. This proves that the signal is not due to X-ray photons but to MeV particles.

We assume that no nuclear processes take place and that no neutrons are formed, and that thus only protons and photons are involved in the signal generation. The small contribution from d + d fusion due to the natural content of d in the hydrogen gas is here neglected. The main results are found by intercepting the beam to the scintillator with the beam-flag or with the inner detector plate. An example of the results found with the full beam flux from the target to the outer detector is shown in Fig. 2. No preamplifier was used in this experiment. The difference signal between the measurements with beam-flag closed and open gives the signal which is removed by the beam-flag. This difference signal does not have the same shape as either of the signals measured. The inset in Fig. 2 shows that an increasing fraction of the signal is removed at increasing TOF in the time range 100–350 ns in the figure, giving a maximum of the signal fraction removed by the beam-flag. This indicates that the difference signal in this time range is due to particles which pass the beam-flag with a probability that decreases with decreasing kinetic energy. It is interesting to note that more than 50% of the peak intensity is passed by the beam-flag which in this case consisted of an 8 mm thick glass plate and 45 μm Al foils. This means that this part of the signal is due to photons which pass through the flag, probably indicating photons with energy above 10 keV. Reflections around the flag edge may of course contribute slightly to the observed signal with closed beam-flag. The signal removed by the beam-flag is mainly due to atomic particles, certainly mainly protons.

To analyze the signal further, the inner detector with its 3 mm wide opening in the steel plate shown in Fig. 1 is rotated into the particle beam from the target to the scintillator, selectively blocking the flux from different parts of the plasma at the target surface. Typical results for the flux to the detector are shown in Figs. 3 and 4. In one position of the inner detector, called blocking here in Fig. 3, the signal to the outer detector is relatively low and not strongly influenced by the beam-flag, presumably since it is mainly due to X-ray photons. The inset in the figure shows a different behavior for the difference signal than in Fig. 2, with a much smaller fraction removed a lower particle energy, probably since no protons exist in the beam flux to the detector in this case. In another position here called transmitting shown in Fig. 4, three degrees (3.8 mm motion for the slit) from the first one, the signal is much stronger with the beam-flag open, and almost completely removed when the beam-flag is closed. This indicates mainly atomic particles, thus protons (and possibly visible photons). A slow signal is however observed in the bump at 200–600 ns in Fig. 4. This indicates protons delayed by collisions in the beam-flag which remove some of their kinetic energy. This beam-flag is here 45 μm Al which means that protons with energy >2 MeV may also penetrate, but a considerable fraction should be scattered and delayed as observed.

At other positions of the inner detector, the signal observed with the outer detector is more complex, as shown in Fig. 5a. This is the behavior observed at angles of the inner detector close to the transmitting position, with the beam-flag closed. This distribution gives the appearance of a photon (X-ray) peak and a delayed proton part of the signal, at approximately 100 ns delay. This behavior can be observed under many different conditions. It can also be observed as in Fig. 5b by just intercepting the flux to the scintillator by moving the inner detector plate (shown in non-blocking position in Fig. 1). This distribution is thus measured with the beam-flag open. It may be noted that the flux in Fig. 5b is delayed further relative to that in Fig. 5a. This is in agreement with the explanation that the particles are delayed by interaction with the inner detector in Fig. 5b, much farther from the scintillator than the beam-flag which gives the delay in Fig. 5a. However, the possibility of multiple collisions in the foils complicates the situation. To prove that the delayed signal does not exist with the beam-flag open, the signal with and without the beam-flag need to be compared directly. In Fig. 6, the signal to the PMT is low enough to allow sequential recording of the signal with closed and open flag with no overloading of the preamplifier. In this case, the delay given by the flag is also clearly seen.

TOF distributions with a clearly delayed peak (bump) are thus easily observed in the experiments with examples in Figs. 3–6. The obvious explanation for this delayed and partly penetrating signal is fast protons. The second peak observed in Fig. 5a corresponds to 700 keV u^{-1} for a particle moving over the entire flight distance from the target. The delayed or scattered particles moving

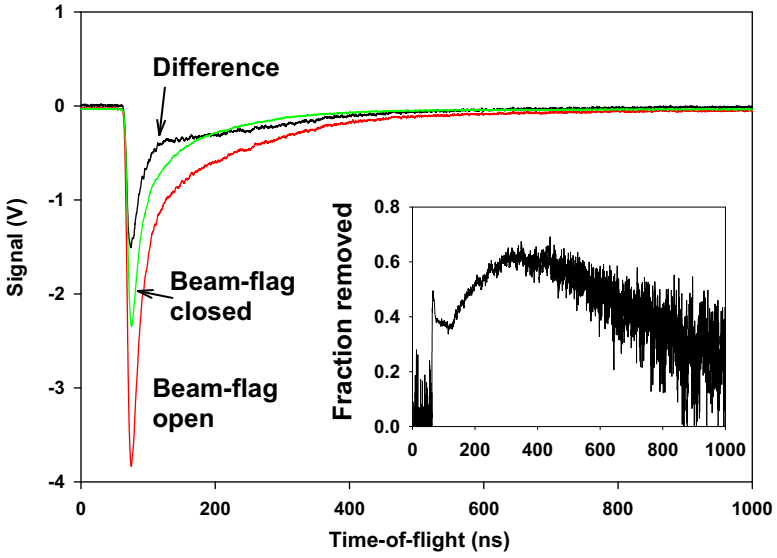

Fig. 2. Signal with the inner movable detector rotated out of the beam. The inset shows the ratio of the difference between the two signals measured with and without the beam-flag to the full signal with no beam-flag. No preamplifier used. Beam-flag was 45 μm Al and 8 mm glass.

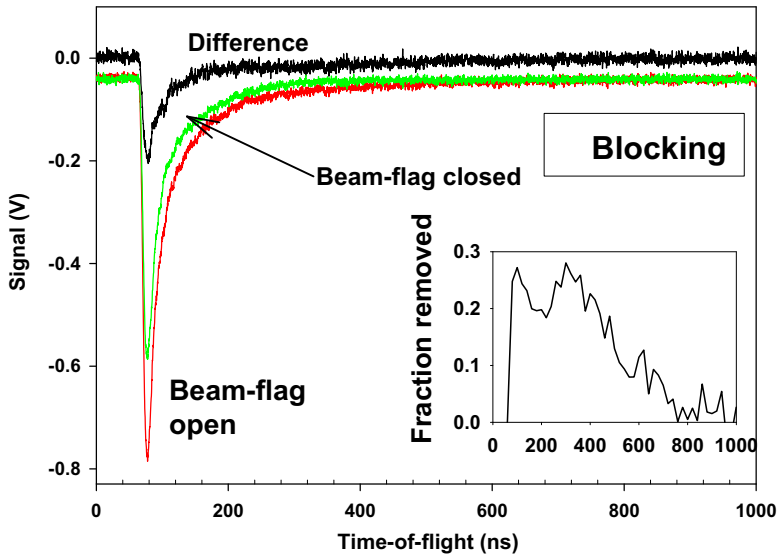

Fig. 3. Signal with the inner detector in a blocking position, giving a small difference between the signals with beam-flag open and closed. The inset shows the (smoothed) ratio of the difference between the two signals measured with and without the beam-flag to the full signal with no beam-flag. No preamplifier used. Beam-flag was 45 μm Al.

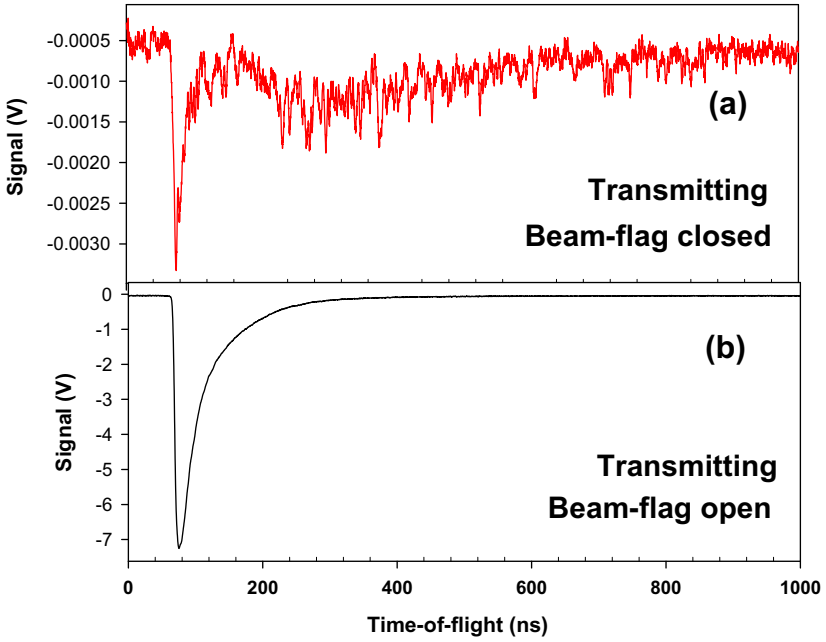

Fig. 4. Signal with the inner detector in a transmitting position 3° (3.8 mm) from the blocking position in Fig. 3, giving a large difference between the signals with beam-flag closed (a) and open (b) in the two panels. No preamplifier used. Beam-flag was 45 μm Al.

from the flag to the scintillator may have lower energy, but they are anyway easily detected in the scintillator. The delayed peak in Fig. 5b corresponds to 250 keV u^{-1} assuming the full flight distance with this energy. The delayed protons can from this be calculated to have >200 keV u^{-1}, while the non-delayed protons have a flight time of the order of 80 ns, corresponding to 1 MeV u^{-1}.

In other cases the particles appear to be much more strongly delayed, like in Fig. 7. Two different cases with the inner detector in different positions from the same experiment are compared there. In Spectrum B, a delay similar to those in Fig. 5 is found, but in Spectrum A, the peak of the delayed signal is much later, at 1.5 μs. Spectrum A agrees well with a thermal distribution at 2.6 keV or 30 MK, while Spectrum B is not thermal. A proton arriving at 6 μs in the figure has a kinetic energy of only 150 eV and should not be detectable. If the signal was caused by high-energy photons formed closer to the laser target for example in the blocking plate, the signal would come even earlier. Thus, the thermal-like distribution Spectrum A is unlikely to have a thermal particle origin caused by the laser pulse. Emission of photons only is also excluded as the source of the thermal-like particle distribution. The only possibility is the emission of high-energy detectable particles from the laser target many μs after the laser pulse. This means that the process giving these high-energy particles is caused by the laser pulse with a considerable delay in the ejection. Thus it may be due to a structural relaxation in the surface layer of dense hydrogen p(1) formed by the laser impact on p(−1). This may give the thermal appearance. This slow distribution is not observed with the blocking plate in a slightly different position as shown

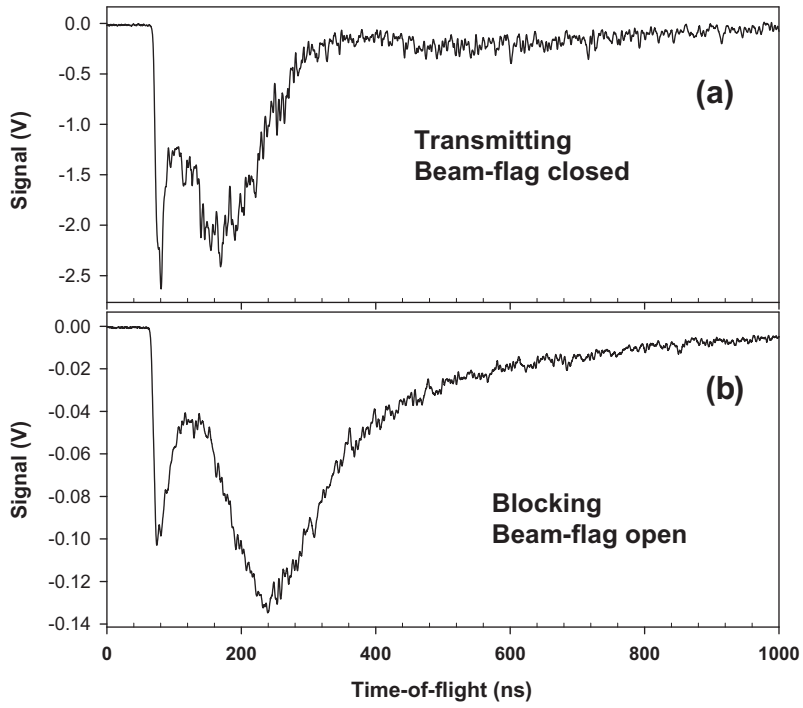

Fig. 5. Delayed signal due to the 45 μm thick Al beam-flag in (a) and due to the inner detector wall (plate) in a blocking position in (b). Preamplifier used in (a) but not in (b).

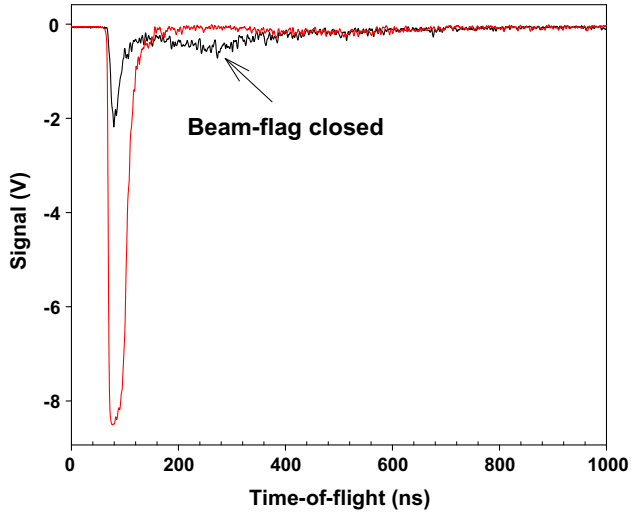

Fig. 6. Delayed signal with beam-flag closed compared to signal with flag open. Beam-flag was 45 μm Al. Preamplifier used.

by Spectrum B in Fig. 7. This may indicate that the high-energy particles are ejected from positions on the target surface far from the laser focus since the slit in the blocking part is in this case far from the normal beam-transmitting position. A weaker flux of particles arrives even with the beam-flag closed in this case, which shows that high-energy particles partially penetrating the flag are emitted several μs after the laser pulse.

The function of the beam-flag may need some verification. Thus, experiments have been done with the outer detector changed, using a dynode–scintillator–PMT ion detection set-up. An example is shown in Fig. 8 with ions formed from $p(-1)$ and accelerated from a vertical laser target with applied voltage of 300 V. Some intense ion peaks are assigned in the figure. (This detector construction has a much lower sensitivity to fast particles in the 100 keV to MeV range.) It is observed that the flux in the ion peaks is removed completely by the beam-flag which means that the flag is dense for the ions with energy <1 keV. However, some delayed intensity leaks through with strong energy loss at longer times both at approximately 4 and >20 μs, probably by scattering around the edge of the flag. Thus the beam-flag works correctly as assumed for the results above.

5. Discussion

The delay of the particles passing through the beam-flag and through the plate in the inner detector can be estimated from the TOF data as described above. The delayed protons were concluded to have >200 keV u^{-1}, while the direct protons have energy of the order of 1 MeV u^{-1}. The signals observed must be due to multiple collisions in the materials, both in transmission and to a small extent in reflections around the edge of the beam-flag. From the PSTAR database [25], the range for protons in the materials used can be estimated. Such data are given in Table 1. Protons with energy of 1 MeV are not expected to penetrate 45 μm Al, which is the typical flag material used. 3 MeV protons will however penetrate to some extent. Since neutrons are excluded in this system where (almost) only protons are introduced, it is concluded that protons of MeV energy are formed by the laser interaction with $p(-1)$.

Below, the problem with afterpulses in the PMT will be discussed first and shown to be of no significance here. After that, a few possibilities to explain the observation of MeV particles will be treated in detail and a conclusion based on all the available information is found.

5.1. Experimental

The preamplifier used in some of the experiments has a bandwidth of 350 MHz and a rise-time of <1 ns which is more than sufficient for correct observation of the photon pulses from the scintillator. There may anyway exist some problems at high overloads. Thus, the experiments have been done avoiding overloads.

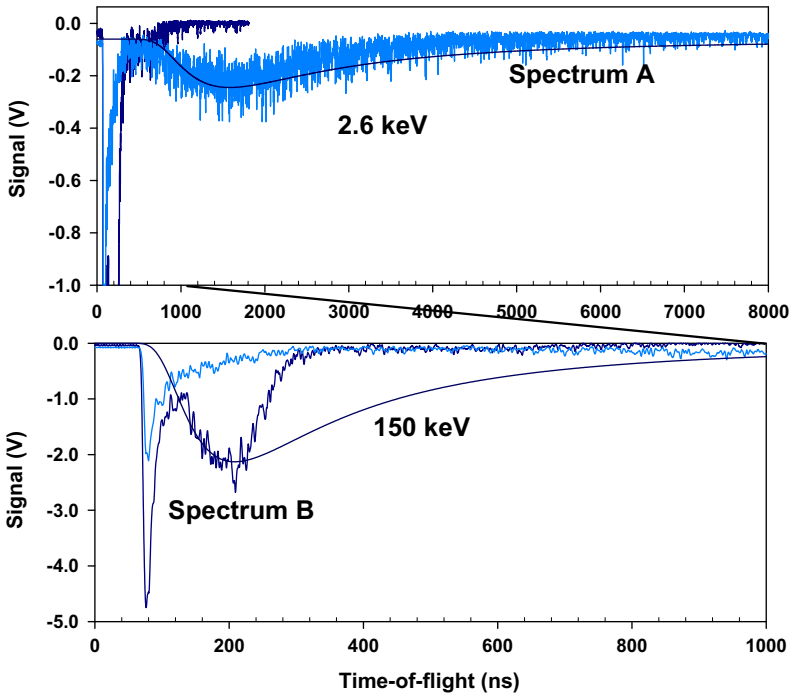

Fig. 7. Delayed signals with beam-flag open at two different positions of the inner blocking detector. The light-blue curve is Spectrum A, and the dark-blue curve is Spectrum B. Preamplifier used. Observe the good fit to a thermal particle distribution for Spectrum A. (For interpretation of the references to color in this figure legend, the reader is referred to the web version of this article.)

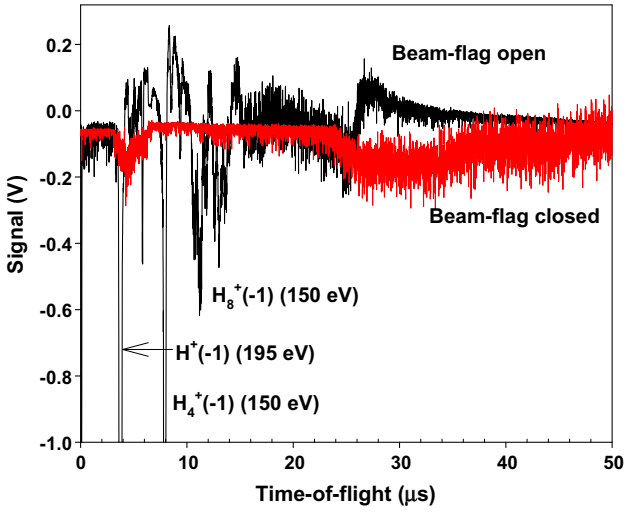

Fig. 8. Signal in the outer detector due to neutral particles from p(−1) (dynode – thin scintillator set-up). Beam-flag was 30 μm Al. The most intense ion peaks are identified, with initial energy of 150–195 eV and an acceleration voltage of 300 V on the laser target. Preamplifier used.

Table 1
Time-of-flight (TOF) in the experiments and ranges for a few energies of protons in the materials used. The databases at NIST [25] are used.

Energy (MeV)	TOF (ns)	Range in p(−1) (nm)	Range in Al (μm)	Range in scintillator (μm)
0.1	256	0.006	0.8	1.3
0.3	148	0.02	3	4
1	80	0.17	15	24
3	47	1.2	82	150

They have also been performed both with and without the preamplifier to ascertain that no artifacts exist. For example, in Fig. 5a the preamplifier is used, while in Fig. 5b it is not used. It is thus safely concluded that the preamplifier does not contribute to the observed delays and other features observed.

Electrons could be emitted by the laser pulse from the target. It is not likely that they have an energy above a few keV [26], since they will be ejected by the relatively weak laser field from the target. No electron signal has been observed in this setup in numerous experiments with laser targets at negative potential. Thus, the electrons ejected are likely to be of low energy, or they may primarily be attached to cluster fragments, giving neutral cluster fragment ejection as normally observed [7,8,10]. If free electrons are ejected with energy of a few keV, they will bend enough in the geomagnetic field to not be able to reach the scintillator at the end of the TOF tube. Stray magnetic fields in the surrounding equipment will also bend the electron trajectories to approach the steel walls where the electrons are lost. Electrons with a few keV of energy will give a very low signal in the scintillator, and will not penetrate far into the scintillator. They will not be able to penetrate through the beam-flag or through the steel plate in the inner detector. Thus, they can be safely disregarded in this experiment.

One artifact that has been carefully checked here is due to so called ion afterpulses in the PMT [27]. Such pulses can appear after intense photon pulses to the PMT, and they can be observed at times 100 ns to several μs after the pulse, varying with the construction of the PMT. For example, for Electron Tubes 9128B the afterpulse rate is specified to be 1%, from 200 ns to 6.4 μs (most PMT manufacturers do not specify anything about afterpulses). This PMT is of the linear focused design, similar to the PMT Electron Tubes 9813B used here. According to our own tests and experience with the actual PMT used, its afterpulses appear at 300–800 ns, often showing a typical structure due to the residual gas ion spectrum in the PMT. A typical case with no such structure but a broad first peak is shown in Fig. 9. The low intensity single-particle peaks at 500–700 ns in the figure are considered to be afterpulses, and they probably appear due to the very high inten-

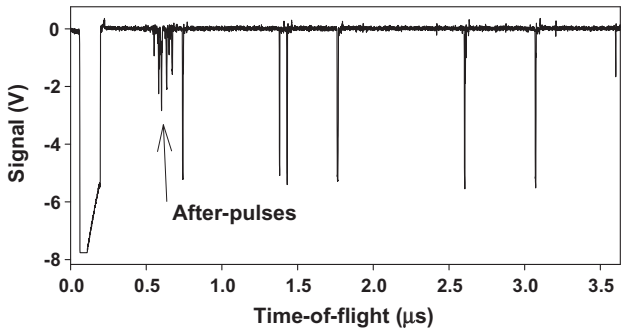

Fig. 9. Demonstration of ion after-pulses in the photomultiplier, with beam-flag open and transmitting inner detector.

sity in the first peak. They are considerable smaller than the ordinary photon pulses shown at later times in Fig. 9. All figures used here for the MeV and delayed peaks are averaged oscilloscope data so that the first peak can be observed directly at its true intensity. The delayed peaks discussed here in Figs. 3–7 are much larger relative to the corresponding first peak than possible for afterpulses, and they are found at shorter times than normally observed for afterpulses. It is concluded that afterpulses in the PMT are not significant for the results obtained.

5.2. Fusion and ponderomotive forces

In ultra-dense deuterium d(−1), specific fast particles are ejected due to laser-induced fusion [1,2]. These earlier studies mainly report on particles delayed by collisions in the ultra-dense material. The initial particles emitted with 1–3 MeV from fusion are not resolved well enough to allow an accurate energy measurement by TOF. Only a small fraction of these particles are in fact observed by the pulse-counting measurements used [1,2]. Using oscilloscope measurements, it becomes clear that a very large number of MeV particles exists. The behavior for p(−1) and d(−1) is similar concerning the very fast particles. Thus, it is expected that a mechanism releasing MeV particles in d(−1) also exists as shown here for p(−1), and this may indeed be one further high-energy mechanism giving rise to the observed nuclear fusion. It is not expected that fusion d + d at the low concentration of d in the natural hydrogen used here will give similar features to those in pure d(−1) and thus that fusion processes will have any importance in the present experiments on H(−1).

Another possibility for high-energy particles from H(−1) could be ponderomotive forces due to the electric field strength in the laser focus. However, the laser intensity of $<10^{12}$ W cm^{-2} used here is much too low to give any such effects. The focusing lens has 400 mm focal length, and the laser pulse is 5 ns long. It is concluded that no such effect can give MeV particles in the present experiments. Further, there exists an induction period in the formation of the fast particles (see further below), and a direct ponderomotive laser interaction is thus completely excluded.

5.3. Stimulated compression

Ultra-dense deuterium d(−1) is observed to be superfluid [11]. Thus, energy transport is fast in this material. The behavior of p(−1) is similar, forming a migrating film of p(−1) on the laser target. When the condensate from the source falls down to the laser target, it contains both forms p(1) and p(−1). When p(1) decays to the state p(−1), a few hundred eV per atom is released in this process. Due to the rapid energy transport in the superfluid material as also described in Section 2, energy pooling may exist which

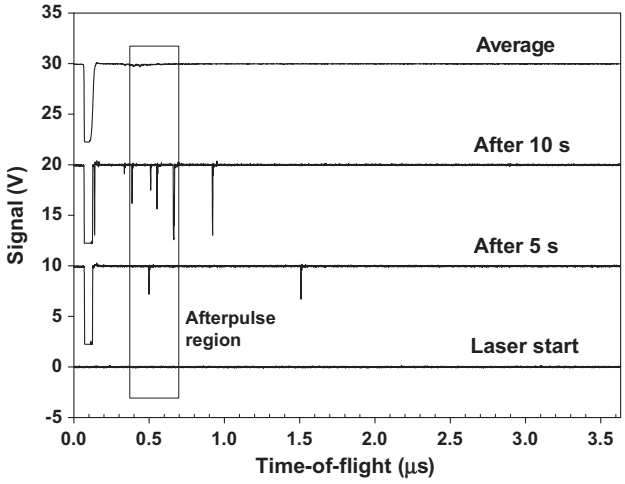

Fig. 10. Induction period for generation of high-energy particles from p(−1), with the outer detector. Beam-flag open, inner detector partially blocking.

means that much higher ejected particle energies may be found. The loss of MeV particles will cool the condensate p(−1) rapidly. We conclude that the most likely process is ejection of MeV protons from the p(−1) phase and that this process gives the observed MeV protons. However, how this process is initiated by the laser pulse must also be understood to make the process complete. With no laser pulse present, the p(−1) state is formed on the metal surface. In order to observe the transition from the p(1) to the p(−1) state, a laser pulse has to first transform the p(−1) material into the p(1) state. This is where the laser energy input is needed.

No high-energy peaks from p(−1) exist during the first laser shots in an experiment as shown in Fig. 10. However, they increase in intensity in 20 s to a steady-state value when the laser is running at 10 Hz repetition rate. If the time between the laser shots is much longer than 100 ms, thus if the repetition rate is lower, the material transferred to p(1) by the laser pulse appears to return back to p(−1) without direct emission of MeV protons. This means that the spontaneous conversion to p(−1) is not enough to eject MeV protons in a short time-frame after the laser pulse, but that a similar laser-driven process exists. Results taken with the inner (ion) detector in the same experiment are shown in Fig. 11. A short induction period is there observed for the ejection of cluster fragments from p(−1), even if the first laser shot does not give any ions in this case either, similar to the result in Fig. 10. Thus, p(−1) exists on the target but the ejection of MeV particles has a longer induction period. This can also be observed from the first MeV peak at 50 ns in Fig. 11, which is still growing even after 10 s with laser impact at 10 Hz repetition rate.

In the CE process in p(−1) induced by the laser pulse, protons are accelerated to energies up to 390 eV, which is the CE energy value found in experiments. This means that fast protons will enter also neighboring p(1) regions (if such exist initially or have been formed by the laser impact in previous laser shots), giving compression and short collisional distances between protons. This may start the transformation (self-compression) to p(−1). The protons may even be captured in close collisions with stationary protons in p(1) due to the exchange force expected to exist for p(−1) as well as for d(−1) [17,18]. Thus, the CE process not only gives excitation of the p(−1) phase to p(1) but is also likely to promote the renewed formation of p(−1) in nearby locations. Of course, that an energy input from the laser beam excites p(−1) to p(1) and at the same time increases the rate of conversion between the two states may be expected and does not require any special properties of the materials. This type of laser-induced compression from p(1) to p(−1) is what is required to give the observed behavior of MeV

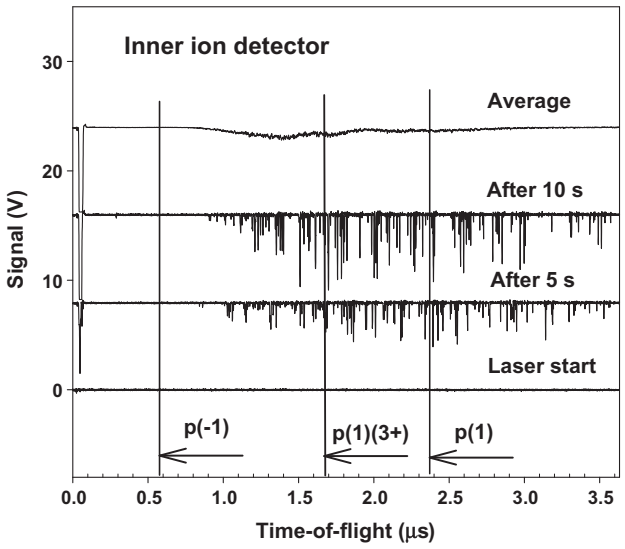

Fig. 11. Short induction period for low-energy ions from p(−1), observed by the inner detector. The shortest TOF for particles from p(−1) and p(1) are shown. p(1)(3+) indicates a CE process with three charges [12].

proton ejection and also to explain its observed dependence on the laser pulse rate, including the considerable induction time.

6. Conclusions

MeV particles are observed by time-of-flight after pulsed laser impact on ultra-dense protium p(−1) films on metal surfaces. The MeV particles ejected are massive as shown by their delay in beam-flags and metal plates and are mainly protons ejected from the superfluid surface phase. No nuclear reactions are expected in this system with (almost) only protons admitted. An induction period of several seconds exists before the MeV protons are ejected. It is concluded that the high kinetic energy is provided by collective self-compression from the state p(1) to p(−1), releasing a few hundred eV per atom. This energy is pooled in the superfluid condensate to a smaller number of protons, giving protons with up to MeV energies. Lower energy keV protons are ejected up to several μs after the laser pulse. The induction period shows that the higher state p(1) must be formed before ejection of MeV particles can start.

References

[1] S. Badiei, P.U. Andersson, L. Holmlid, Laser Part. Beams 28 (2010) 313.
[2] P.U. Andersson, L. Holmlid, J. Fusion Energy (2012) in print, doi: 10.1007/s10894-011-9468-2.
[3] S. Badiei, P.U. Andersson, L. Holmlid, Int. J. Hydrogen Energy 34 (2009) 487.
[4] S. Badiei, P.U. Andersson, L. Holmlid, Int. J. Mass Spectrom. 282 (2009) 70.
[5] P.U. Andersson, L. Holmlid, Phys. Lett. A 373 (2009) 3067.
[6] L. Holmlid, H. Hora, G. Miley, X. Yang, Laser Part. Beams 27 (2009) 529.
[7] S. Badiei, P.U. Andersson, L. Holmlid, Phys. Scr. 81 (2010) 045601.
[8] P.U. Andersson, L. Holmlid, Phys. Lett. A 374 (2010) 2856.
[9] S. Badiei, P.U. Andersson, L. Holmlid, Appl. Phys. Lett. 96 (2010) 124103.
[10] P.U. Andersson, B. Lönn, L. Holmlid, Rev. Sci. Instrum. 82 (2011) 013503.
[11] P.U. Andersson, L. Holmlid, Phys. Lett. A 375 (2011) 1344.
[12] L. Holmlid, Int. J. Mass Spectrom. 304 (2011) 51.
[13] L. Holmlid, J. Cluster Sci. (2012) in print, doi: 10.1007/s10876-011-0387-1.
[14] V. Komarov, T. Azaryan, D. Chiladze, et al., Phys. Rev. Lett. 101 (2008) 102501.
[15] S. Dymov, V. Komarov, G. Macharashvili, et al., Phys. Rev. C 81 (2010) 044001.
[16] T. Guénault, Basic Superfluids, Taylor and Francis, London, 2003.
[17] F. Winterberg, J. Fusion Energy 29 (2010) 317.
[18] F. Winterberg, Phys. Lett. A 374 (2010) 2766.
[19] L. Holmlid, submitted for publication.
[20] S. Badiei, L. Holmlid, J. Phys.: Condens. Matter 16 (2004) 7017.
[21] S. Badiei, L. Holmlid, J. Phys. B: At. Mol. Opt. Phys. 39 (2006) 4191.
[22] L. Holmlid, J. Nanopart. Res. 13 (2011) 5535.
[23] G.R. Meima, P.G. Menon, Appl. Catal. A 212 (2001) 239.
[24] M. Muhler, R. Schlögl, G. Ertl, J. Catal. 138 (1992) 413.
[25] National Institute of Standards and Technology NIST, Physics Laboratory, PSTAR program.
[26] L. Torrisi, S. Gammino, Nucl. Instr. Meth. B 243 (2006) 143.
[27] P.B. Coates, J. Phys. D: Appl. Phys. 6 (1973) 1159.